

Article

Induction Motor DTC Performance Improvement by Inserting Fuzzy Logic Controllers and Twelve-Sector Neural Network Switching Table

Chaymae Fahassa ¹, Yassine Zahraoui ¹, Mohammed Akherraz ¹, Mohammed Kharrich ^{1,*}, Ehab E. Elattar ²
and Salah Kamel ^{3,*}

- ¹ Department of Electrical Engineering, Mohammadia School of Engineering, Mohammed V University, Rabat 10090, Morocco; fahassa.chaymae@gmail.com (C.F.); yassinezahraoui@research.emi.ac.ma (Y.Z.); akherraz@emi.ac.ma (M.A.)
- ² Department of Electrical Engineering, College of Engineering, Taif University, Taif 21944, Saudi Arabia; e.elattar@tu.edu.sa
- ³ Department of Electrical Engineering, Faculty of Engineering, Aswan University, Aswan 81542, Egypt
- * Correspondence: mohammedkharrich@research.emi.ac.ma (M.K.); skamel@aswu.edu.eg (S.K.)

Abstract: Human civilization has changed forever since induction motors were invented. Induction motors are widely used and have become the most prevalent electrical components due to their beneficial characteristics. Many control strategies have been developed for their performance improvement, starting from scalar to vector to direct torque control. The latter, which is a class of vector control, was proposed as an alternative to ensure separate flux and torque control while remaining completely in a stationary reference frame. This technique allows direct inverter switching and reasonable simplicity compared to other vector control techniques, and it is less sensitive to parameter variation. Yet, the use of hysteresis controllers in conventional DTC involves undesired ripples in the stator current, flux, and torque, which lead to bad performances. This paper aims to minimize the ripple level and ensure the system's performance in terms of robustness and stability. To generate the appropriate reference control voltages, the proposed method is an improved version of DTC, which combines the power of fuzzy logic, neural networks, and an increased number of sectors. Satisfactory results were obtained by numerical simulation in MATLAB/Simulink. The proposed method was proven to be a fast dynamic decoupled control that robustly responds to external disturbance and system uncertainties.

Keywords: induction motor drive; fuzzy logic control; neural network switching table; twelve-sector DTC; total harmonic distortion; flux distortion; torque and current pulsation; harmonic reduction

MSC: 92B20; 68T40; 93C42



Citation: Fahassa, C.; Zahraoui, Y.; Akherraz, M.; Kharrich, M.; Elattar, E.E.; Kamel, S. Induction Motor DTC Performance Improvement by Inserting Fuzzy Logic Controllers and Twelve-Sector Neural Network Switching Table. *Mathematics* **2022**, *10*, 1357. <https://doi.org/10.3390/math10091357>

Academic Editors: José Carlos R. Alcántud and Gustavo Santos-García

Received: 11 March 2022

Accepted: 15 April 2022

Published: 19 April 2022

Publisher's Note: MDPI stays neutral with regard to jurisdictional claims in published maps and institutional affiliations.



Copyright: © 2022 by the authors. Licensee MDPI, Basel, Switzerland. This article is an open access article distributed under the terms and conditions of the Creative Commons Attribution (CC BY) license (<https://creativecommons.org/licenses/by/4.0/>).

1. Introduction

The trajectory of human history has changed since the invention of induction motors. Even today, this century-old motor, firstly designed by the famous Nicola Tesla, is the most widespread motor type. Induction motors consume around half of all global electric power. They are built and designed for empirical simplicity, unlike any other electrical equivalent; permanent magnets are not needed; most are brush-less; they have no commutator rings or position sensors [1]. Induction motors are also self-starting; they do not need a mover or exciter to start-up. Their speed can be easily controlled by modifying the power frequency, and this is the most significant advantage of induction motors. They are suitable for elevators, cranes, and especially, electric cars [2]. Electric vehicles can operate with a single-speed transmission due to the high-speed range of induction motors. Another noteworthy feature is that they can also work as a generator; in this case, a prime mover is mandatory to move the rotor at start-up. Thus, it is obligatory to ensure that the speed of the rotor is always higher than the rotating magnetic speed [3].

Vector control, also known as field-oriented control (FOC), was developed to overcome the limitations of scalar control. The FOC approach was introduced in the 1970s, designed to establish autonomous torque and flux control comparable to DC machines (separate excitation) [4]. It has some drawbacks; one of its fundamental drawbacks is the coordinates' transformation. This transformation requires the flux angle, which cannot be directly measured because it is difficult to place a flux sensor in the air gap of the machine. Another drawback is related to the machine's sensitivity to parameter variation such as stator and rotor resistance [5]. Meanwhile, direct torque control (DTC) is another way that ensures separated and decoupled flux and torque control. This technique was introduced for the first time by Takahashi and Noguchi in Japan in the middle of the 1980s. Unlike FOC, this control strategy is carried out entirely in a stationary frame (coordinates fixed to the stator) [6]. Moreover, DTC produces the gating signals of the inverter directly by the look-up switching table and does not require any modulation such as PWM [7]. Although DTC has fewer model parameters than FOC, it provides a better torque and flux response. In other words, DTC is simpler and has a profoundly fast response. Hence, it is suitable for high-performance drive applications [8,9].

Unfortunately, hysteresis in the fundamental DTC method causes undesired ripples in the flux, current, and torque waveform. Some DTC modifications and improvements have been made, aiming to make the ripples smooth [10,11]. When the artificial neural networks were proposed as an alternative solution to this issue, the study results proved their functionality. Despite its complexity, this intelligent method reduces the high level of ripples by acting on the inverter switching state [12]. Meanwhile, the number of sectors to produce the control voltages of reference is also considered effective to tackle this problem. The study findings showed that twelve-sector DTC results in good dynamics while the system is operated in the high- and low-speed ranges [13,14]. In summary, the proposed approach combines the advantages of both FOC and DTC, and the goal is to eliminate their drawbacks.

Due to the artificial intelligence methods', such as neural networks, fuzzy logic [15], and genetic algorithms, benefits, the performance of AC drives' operation is enhanced. An NN controller is a set of nonlinear functions to establish, by learning, a large number of models and nonlinear connectors [16].

This research aims to control and improve the performance of the induction motor drive by modifying DTC using a robust and nonlinear technique. The research can be summarized as four stages:

- The high torque and flux ripples are minimized by replacing the conventional switching table with an intelligent one based on the ANN algorithm. The number of ripples in the flux, current, and torque can then be reduced.
- After the ripple's reduction, the robustness and stability are addressed.
- Since the number of sectors is the most influential factor to overcome disturbance and system uncertainties, the number of sectors was increased from six to twelve, and a fuzzy logic speed controller was inserted.
- Eventually, a fast dynamic decoupled control that robustly responds to external disturbances and system uncertainties can be achieved.

The remainder of this paper is organized as follows. In Section 2, the state space mathematical model of the induction motor is introduced with the start-up speed and torque waveforms. The basic DTC control law of the induction motor is presented in detail in Section 3. In Section 4, the twelve-sector technique for DTC performance improvement is explained. After that, the fuzzy logic control design is illustrated in Section 5. Then, Section 6 highlights the artificial neural network switching table in detail. In Section 7, the simulation results of the proposed twelve-sector ANN-DTC are presented and discussed. The conclusions of the paper are given in Section 8.

2. Induction Motor State Space Mathematical Model

The representation of the state space model can be mathematically written as:

$$\begin{cases} \dot{X} = \mathbf{A}X + \mathbf{B}U \\ Y = \mathbf{C}X \end{cases} \quad (1)$$

X : state vector; U : input vector; Y : output vector. According to [17], the state and the input vectors of an induction motor can be defined by the stator current and rotor flux components based on their α - β stationary coordinates. Thus, they can be defined as: $X = [i_{s\alpha}, i_{s\beta}, \phi_{r\alpha}, \phi_{r\beta}]^T$; $U = [v_{s\alpha}, v_{s\beta}]^T$; $Y = [i_{s\alpha}, i_{s\beta}]^T$.

$i_{s\alpha}$ and $i_{s\beta}$ are components of the stator current α - β reference frame. $\phi_{r\alpha}$ and $\phi_{r\beta}$ are the components of the rotor flux. $v_{s\alpha}$ and $v_{s\beta}$ are the components of the stator voltage in α - β . Therefore, the components of the matrices in the state space representation can be obtained by analyzing the differential equations of the rotor flux and stator current, as in the matrices below.

$$\mathbf{A} = \begin{bmatrix} -\lambda & 0 & \frac{K}{T_r} & K\omega_r \\ 0 & -\lambda & -K\omega_r & \frac{K}{T_r} \\ \frac{L_m}{T_r} & 0 & -\frac{1}{T_r} & -\omega_r \\ 0 & \frac{L_m}{T_r} & \omega_r & -\frac{1}{T_r} \end{bmatrix};$$

$$\mathbf{B} = \begin{bmatrix} \frac{1}{\sigma L_s} & 0 \\ 0 & \frac{1}{\sigma L_s} \\ 0 & 0 \\ 0 & 0 \end{bmatrix}; \mathbf{C} = \begin{bmatrix} 1 & 0 & 0 & 0 \\ 0 & 1 & 0 & 0 \end{bmatrix}$$

$$\lambda = \frac{R_s}{\sigma L_s} + \frac{1-\sigma}{\sigma T_r}; K = \frac{1-\sigma}{\sigma L_m}; \sigma = 1 - \frac{L_m^2}{L_s L_r}; T_r = \frac{L_r}{R_r}.$$

R_s : resistance of the stator; R_r : resistance of the rotor; L_s : inductance of the stator; L_r : inductance of the rotor; L_m : mutual inductance; T_r : time constant of the rotor.

Figure 1 demonstrates the block diagram of the induction motor state space mathematical model, while Figure 2 shows the start-up mechanical speed and electromagnetic torque waveforms of the above model according to a three-phase 220 V rms.

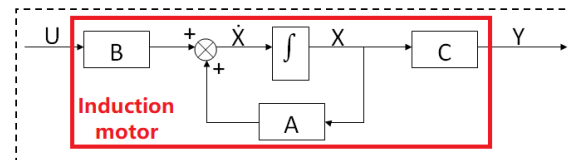


Figure 1. Mathematical model of the induction motor: state space.

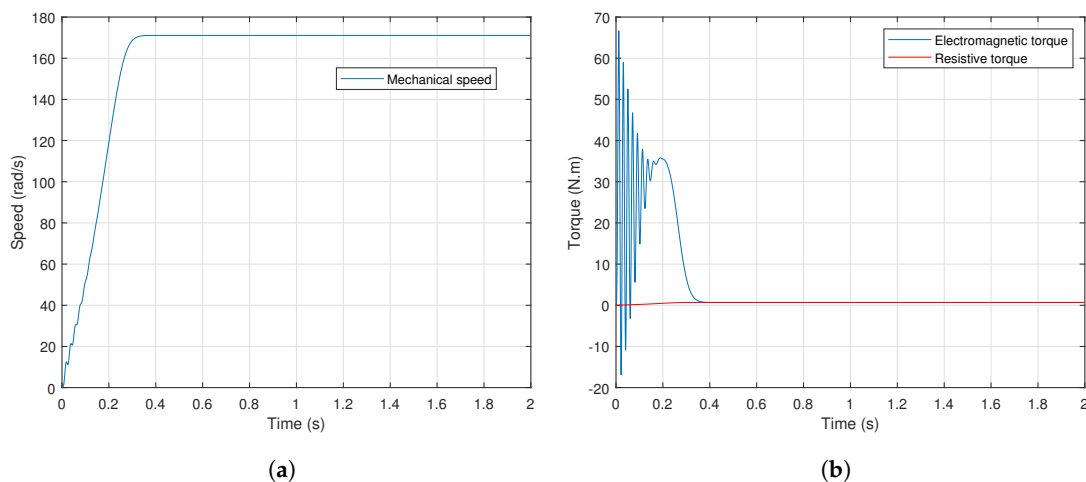


Figure 2. Start-up and steady-state of the induction motor. (a) Start-up: mechanical speed; (b) start-up: electromagnetic torque.

3. Direct Torque Control Basis

The DTC method is used generally in variable-frequency drives in order to control their torque directly, which means consequently and indirectly controlling the speed of AC electric machines (three-phase). This implies computing the estimate of the machine’s magnetic flux and the torque, which are based, respectively, on the measured current and voltage components [18].

3.1. Stator Flux and Torque Estimation

Stator flux estimation is established by combining the stator voltages. Electromagnetic torque is the product of the estimated stator flux components and measured machine current components. The estimated flux magnitude and torque are then compared with their reference values. If either the estimated flux or torque diverges too far from the reference tolerance, the switches of the variable frequency drive are switched off and on in such a way that the flux and torque errors will return to their tolerance bands as quickly as possible. Therefore, direct torque control is classified as hysteresis control [19]. The stator flux can then be written as:

$$\bar{\phi}_s = \int_0^t (\bar{V}_s - R_s \bar{I}_s) dt \tag{2}$$

The α - β coordinates of the stator flux components can be defined as:

$$\phi_{s\alpha} = \int_0^t (v_{s\alpha} - R_s i_{s\alpha}) dt \tag{3}$$

$$\phi_{s\beta} = \int_0^t (v_{s\beta} - R_s i_{s\beta}) dt \tag{4}$$

The flux module can be calculated based on the flux components, which can be mathematically defined as:

$$\phi_s = \sqrt{\phi_{s\alpha}^2 + \phi_{s\beta}^2} \tag{5}$$

Meanwhile, the electromagnetic torque is calculated as the difference of the product of the stator current and flux between different frames, as in the following equation:

$$T_e = p(i_{s\beta}\phi_{s\alpha} - i_{s\alpha}\phi_{s\beta}) \tag{6}$$

3.2. Switching State Vector

Errors that result from the difference between the reference values and estimated values of the stator flux linkage and electromagnetic torque are the inputs to the hysteresis comparators. The outputs of these controllers and the stator flux location determine the input of the switching table. The selector then generates a suitable switching state vector [20]. The conventional DTC switching table is illustrated in Table 1.

Table 1. Basic DTC switching table.

$\Delta\phi_s$	ΔT_e	S_1	S_2	S_3	S_4	S_5	S_6
1	1	110	010	011	001	101	100
	0	111	000	111	000	111	000
	-1	101	100	110	010	011	001
0	1	010	011	001	101	100	110
	0	000	111	000	111	000	111
	-1	001	101	100	110	010	011

This switching state vector ($S_a S_b S_c$) can generate eight position vectors, which are ($\vec{V}_1 \vec{V}_2 \dots \vec{V}_8$), where two of them are null vectors ($S_a S_b S_c$) = (1 1 1) or (0 0 0).

4. Twelve-Sector DTC Algorithm

In the six conventional sectors of DTC, we find two switching states per sector, which are \vec{V}_i and \vec{V}_{i+3} , which are not considered. Thus, the torque control is ambiguous. To fix this situation, a sector shifting is needed. The first sector will be located in $[0 \frac{\pi}{3}]$ instead of $[\frac{11\pi}{6} \frac{\pi}{6}]$. However, in a similar way, this new distribution has also two unused vectors per sector (i.e., \vec{V}_{i+2} and \vec{V}_{i-1}), which this time creates an ambiguity in the flux rather than the torque. Therefore, another strategy was developed for this purpose. The idea is to divide the circular flux into twelve sectors rather than six. Consequently, each sector uses all six states and the ambiguity in torque and flux control can then be avoided [21].

In the twelve-sector DTC, \vec{V}_1 generates a large increase in the flux linkage and a small increase in the torque for Sector 12. On the other hand, \vec{V}_2 results in a large increase in torque and a small increase in flux. Therefore, the variations of small and large torque must now be defined. As a result of this concept, the hysteresis band of the torque is divided into four. Hence, the proposed twelve-sector DTC switching table is provided in Table 2.

Table 2. Switching table of the proposed twelve-sector DTC.

$\Delta\phi_s$	ΔT_e	S ₁	S ₂	S ₃	S ₄	S ₅	S ₆	S ₇	S ₈	S ₉	S ₁₀	S ₁₁	S ₁₂
1	2	\vec{V}_2	\vec{V}_3	\vec{V}_3	\vec{V}_4	\vec{V}_4	\vec{V}_5	\vec{V}_5	\vec{V}_6	\vec{V}_6	\vec{V}_1	\vec{V}_1	\vec{V}_2
	1	\vec{V}_2	\vec{V}_2	\vec{V}_3	\vec{V}_3	\vec{V}_4	\vec{V}_4	\vec{V}_5	\vec{V}_5	\vec{V}_6	\vec{V}_6	\vec{V}_1	\vec{V}_1
	−1	\vec{V}_1	\vec{V}_1	\vec{V}_2	\vec{V}_2	\vec{V}_3	\vec{V}_3	\vec{V}_4	\vec{V}_4	\vec{V}_5	\vec{V}_5	\vec{V}_6	\vec{V}_6
	−2	\vec{V}_6	\vec{V}_1	\vec{V}_1	\vec{V}_2	\vec{V}_2	\vec{V}_3	\vec{V}_3	\vec{V}_4	\vec{V}_4	\vec{V}_5	\vec{V}_5	\vec{V}_6
0	2	\vec{V}_3	\vec{V}_4	\vec{V}_4	\vec{V}_5	\vec{V}_5	\vec{V}_6	\vec{V}_6	\vec{V}_1	\vec{V}_1	\vec{V}_2	\vec{V}_2	\vec{V}_3
	1	\vec{V}_4	\vec{V}_4	\vec{V}_5	\vec{V}_5	\vec{V}_6	\vec{V}_6	\vec{V}_1	\vec{V}_1	\vec{V}_2	\vec{V}_2	\vec{V}_3	\vec{V}_3
	−1	\vec{V}_5	\vec{V}_5	\vec{V}_6	\vec{V}_6	\vec{V}_1	\vec{V}_1	\vec{V}_2	\vec{V}_2	\vec{V}_3	\vec{V}_3	\vec{V}_4	\vec{V}_4
	−2	\vec{V}_5	\vec{V}_6	\vec{V}_6	\vec{V}_1	\vec{V}_1	\vec{V}_2	\vec{V}_2	\vec{V}_3	\vec{V}_3	\vec{V}_4	\vec{V}_4	\vec{V}_5

Several studies have stated that the increase of the sector number slightly reduces the high ripples and current harmonics [22].

5. Fuzzy Logic Control for Speed Loop Regulation

Fuzzy logic control is used broadly in AC machine control. In fact, The term fuzzy relies on the logic engaged being able to deal with the information that we cannot express as true or false, but instead, as partially true. In spite of the fact that alternative techniques such as genetic algorithms (GAs) and neural networks (ANNs) can be carried out exactly as well as fuzzy logic, fuzzy logic has an advantage, whereby the solutions to the problems can be simulated in terms that are understandable by human operators, such that by their experience, the regulator can be designed. This makes it easier to automate the tasks that are currently executed by humans [23].

The fuzzy control system is an intelligent system that is based on fuzzy logic. It is a mathematical system that examines the input in terms of logical variables taken on continuous values, which are between 0 and 1. Error $\varepsilon_\omega = \varepsilon_{i_{sr}} \hat{\phi}_{r\beta} - \varepsilon_{i_{s\beta}} \hat{\phi}_{r\alpha}$ and error variation $\Delta\varepsilon_\omega = \varepsilon_{\omega k} - \varepsilon_{\omega k-1}$ are then considered as fuzzy input variables of the fuzzy controller, whose fuzzy output will generate the variation of the controlled speed $\Delta\hat{\omega}_r = \hat{\omega}_k - \hat{\omega}_{k-1}$. Figure 3 illustrates the structure of the speed loop fuzzy controller.

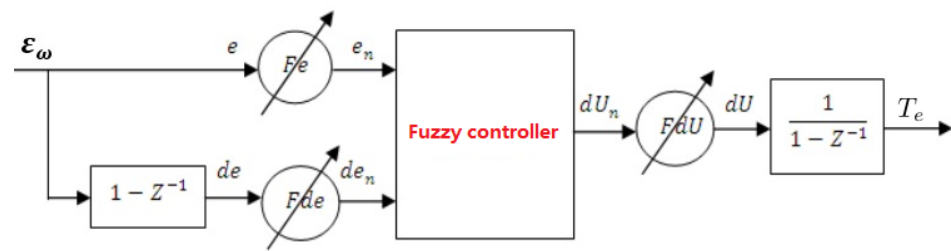


Figure 3. Block diagram: speed regulator with fuzzy logic.

5.1. Fuzzification

The input variables are converted into fuzzy ones and are translated into linguistic labels. The membership functions linked to each label are chosen in triangular forms. The input and the controlled output linguistic variables’ fuzzification is achieved by symmetric triangular membership functions on a universe of speech normalized on the interval $[-1,+1]$ for each variable, as shown in Figure 4.

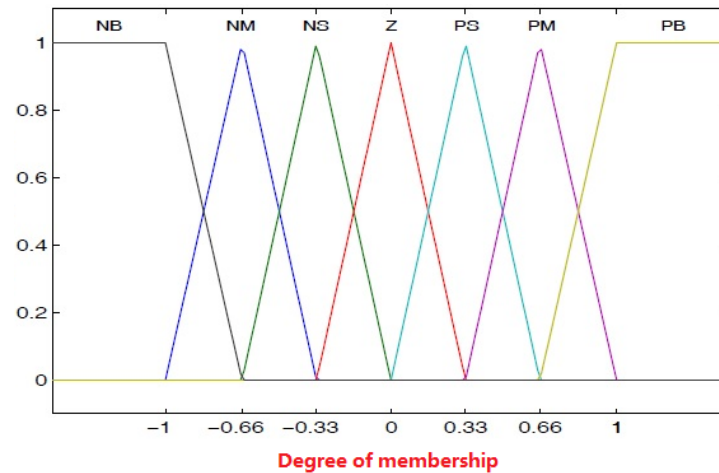


Figure 4. Input and output membership functions of the fuzzy controller.

N means negative, P positive, B big, M medium, S small, and Z zero. NB means negative big; it is the first membership function. The triangular membership functions in fuzzy control lead to a good linguistic classification that has positive effects on operational and control decisions.

5.2. Knowledge Base and Inference Engine

The knowledge base contains the data and the rules base. The data supplies the information that is used to interpret the linguistic rules and the fuzzy data. The rules base states the control goal actions by means of the linguistic control rules set. The inference engine assesses the IF-THEN set and carries out 7×7 rules. The following example shows a linguistic rule form: IF ϵ_ω is NB and $\Delta\epsilon_\omega$ is NB, THEN T_e is NB. Moreover, the inference rules used to determine the output variable based on the input ones are summarized in Table 3.

Table 3. Inference matrix of the fuzzy controller.

$\Delta\epsilon_\omega \backslash \epsilon_\omega$	NB	NM	NS	Z	PS	PM	PB
PB	Z	PS	PM	PB	PB	PB	PB
PM	NS	Z	PS	PM	PB	PB	PB
PS	NM	NS	Z	PS	PM	PB	PB
Z	NB	NM	NS	Z	PS	PM	PB
NS	NB	NB	NM	NS	Z	PS	PM
NM	NB	NB	NB	NM	NS	Z	PS
NB	NB	NB	NB	NB	NM	NS	Z

5.3. Defuzzification

In this phase, the fuzzy variables are transformed into crisp variables. There are many defuzzification strategies to generate the fuzzy set value for the output fuzzy variable. In this paper, the center of gravity defuzzification method is used and the Mamdani algorithm inference technique is utilized. In this case, the center of gravity abscissa corresponding to the fuzzy regulator output of the Mamdani type is given by the following relation:

$$dT_e = \frac{\int x\mu_R(x)dx}{\int \mu_R dx} \tag{7}$$

Each fuzzy controller has three tuning gains; their values are determined by trial and error. This technique consists of performing repetitive tests and tuning each gain separately from the others to view its effect.

6. Artificial Neural Network Switching Table for DTC Performance Improvement

6.1. Artificial Neural Network Structure

Artificial neural networks are generally called neural networks (NNs). They are computing systems based on the biological neural networks that constitute animal brains. The ANN is a series of connected units and nodes called artificial neurons, imitating the neurons in the biological brain. An artificial neuron takes a signal and processes it. The signal at each connection is a real number; likewise, the output of each neuron is calculated by some nonlinear function of the sum of its inputs [24,25].

6.2. Artificial Neural Network Architecture

Artificial neural networks have many architectures, but the typical one is the multilayer feed-forward network using an error back-propagation algorithm. The neural network has three layers: (1) input, (2) hidden, and (3) output layers. Each layer has several neurons. The number of neurons in the input and the output layers is based on the number of input and output variables selected. The number of hidden layers and the number of neurons in each depend on the desired degree of precision [26,27].

6.3. The Proposed ANN Switching Table Architecture

The proposed twelve-sector DTC-NN consists of replacing the switching table that generates the voltage vectors. The input of the NN controller is the α - β control voltages. This NN is based on feed-forward back-propagation with four hidden layers having 4, 14, 16, and 3 neurons in each layer, respectively, and logsig is the activation function. The output layer has three neurons providing the voltage vector, the proposed ANN switching table. The structure of the neural network is used to perform twelve-sector DTC, which is applied to an induction motor, that is a neural network controller with three linear input nodes, thirty-seven neurons in the hidden layer, and three neurons in the output layer. Figure 5 shows the internal structure of the neural network controller, while the architecture of the first layer is shown in Figure 6.

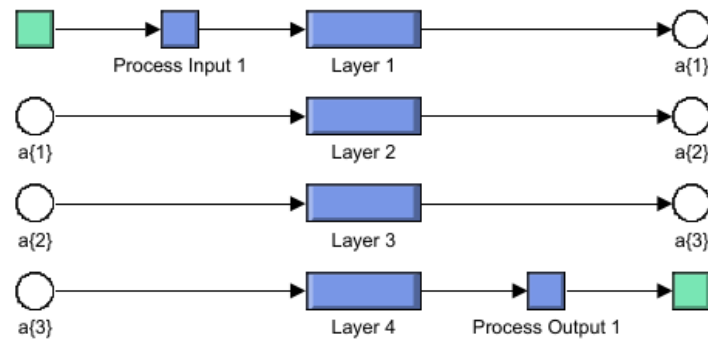


Figure 5. Twelve-sector DTC multilayer neural network architecture.

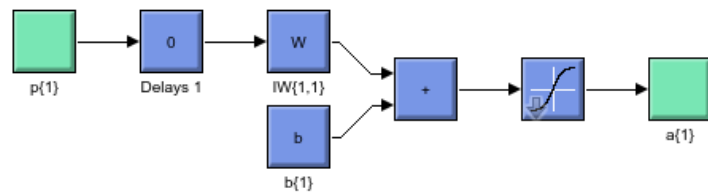


Figure 6. Layer 1 architecture.

The diagram of torque and flux control is based on the proposed twelve-sector DTC with the ANN algorithm and is presented in Figure 7.

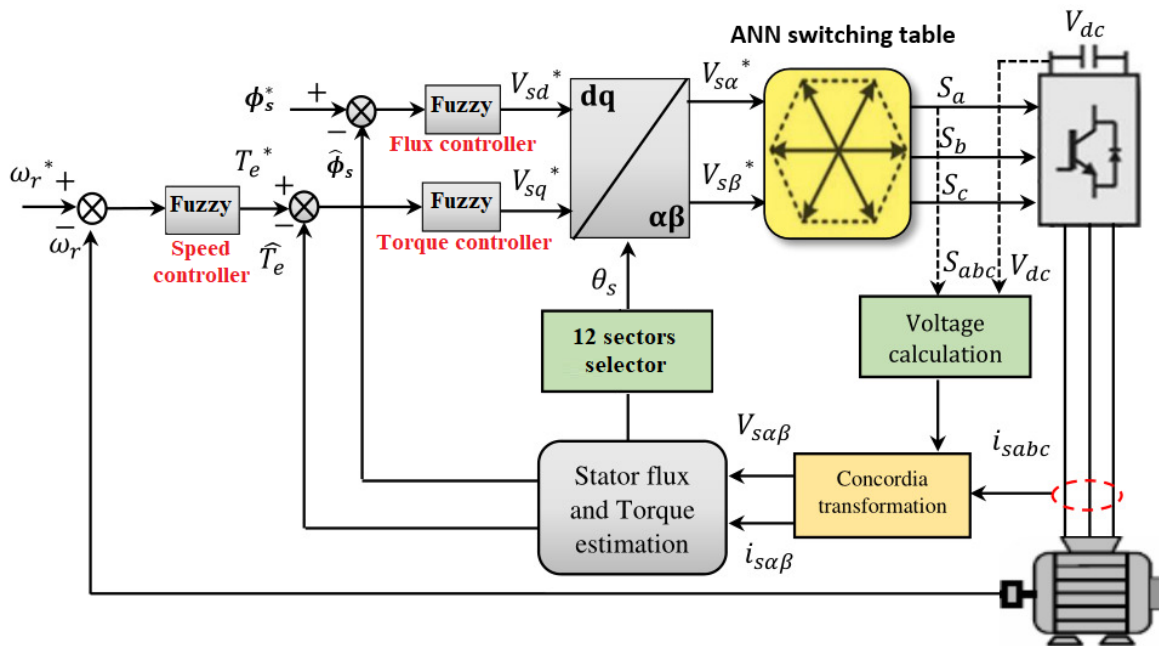


Figure 7. The proposed control scheme. The asterisk * designates the reference quantities.

The speed controller generates the reference torque, while the flux and torque controllers generate the d - q voltage components. The NN switching table generates the inverter control states. In the DTC scheme, there is no need for a PWM modulator, nor the coordinates' transformation. The twelve-sector selector generates the suitable angle for the ANN switching table.

7. Results and Discussion

A comparison of the classical DTC and the twelve-sector fuzzy ANN-DTC is presented in the paper. In MATLAB/Simulink, DTC control algorithms for the three-phase 3 kW squirrel-cage induction motor drive were simulated. Table A1 in Appendix A lists the rated power and the parameters of the induction motor used in this simulation study. The ANN switching table was implemented using the Simulink ANN toolbox.

The test in Figure 8 presents the start-up of the induction motor according to a speed step of 100 rad/s. Then, a load of 10 N·m was applied at $t_1 = 0.8$ s and removed at $t_2 = 1.6$ s.

Both techniques had good performance when starting up, as shown in Figure 8a,b. The applied load disturbance was quickly rejected by the speed regulation loop. The proposed ANN-DTC in Figure 8b shows a better speed response compared to the conventional DTC in Figure 8a. The transient response was not identical in both schemes because the speed controllers' structures were different. We can clearly notice the robustness of the fuzzy speed controller.

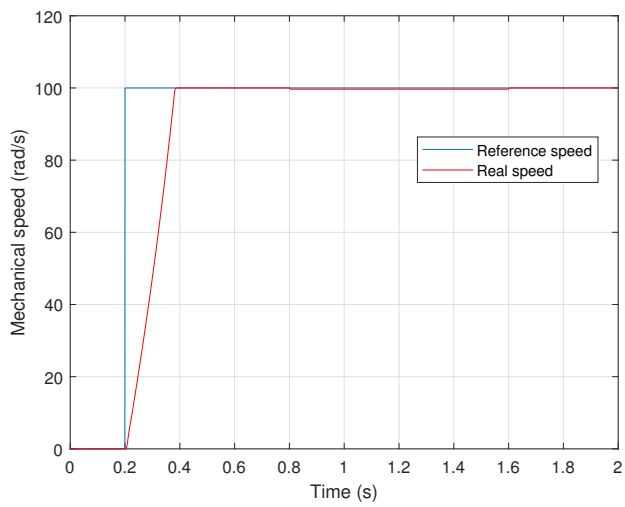
Next, the load-applied responses of the torque are illustrated. The speed controller initially operates the system at its physical limit. Compared to the conventional DTC in Figure 8c, where the high torque ripples exceed the hysteresis bound, the modified DTC-based electromagnetic torque control performance in Figure 8d has a reduced level of ripples due to the use of the ANN. Moreover, according to Figure 9, the proposed ANN-DTC has a lower THD level (47.79%) in Figure 9d compared to the conventional DTC (68.75%) in Figure 9c.

The analysis and observations of the stator flux are highlighted briefly in the following. Both the conventional DTC and the proposed ANN-DTC showed sinusoidal waveforms in their flux responses. However, the conventional DTC in Figure 8e shows a ground sinusoidal curve of stator flux, which designates the high ripple level, while the ANN-DTC in Figure 8f shows a smoother one. This can be explained in Figure 9, where the proposed ANN-DTC has a lower THD level (71.28%) as in Figure 9b compared to the conventional DTC (97.16%) in Figure 9a.

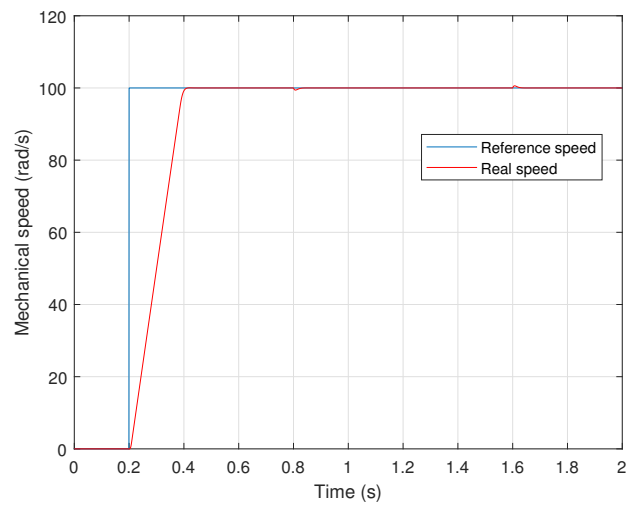
Both the conventional DTC and the proposed ANN-DTC showed sinusoidal waveforms in their stator phase current. However, the conventional DTC in Figure 8g shows a high magnitude sinusoidal waveform, which designates the high ripple level, while the ANN-DTC in Figure 8h shows a lower one. This can be explained in Figure 9, where the proposed ANN-DTC has a lower THD level (19.68%) as in Figure 9f compared to the conventional DTC (34.63%) in Figure 9e.

The stator flux evolution, such as its magnitude and circular trajectory, can also be observed in the simulation results. For example, according to the stator flux magnitude, the ripples exceeded the hysteresis bounds, which can be seen in Figure 8i. Moreover, due to the changing of the zone, the flux initially took a few steps before achieving the reference flux magnitude (1 Wb) (Figure 8k). Furthermore, the stator flux components showed an acceptable waveform, but a high level of ripples. The proposed ANN-DTC showed a reduced level of flux harmonics, quicker magnitude tracking at the initial state, and a better component curve than the classical DTC. This was due to the better zone selection operation of the stator flux vector in the proposed technique. The zone selection operation can be seen in Figure 8l.

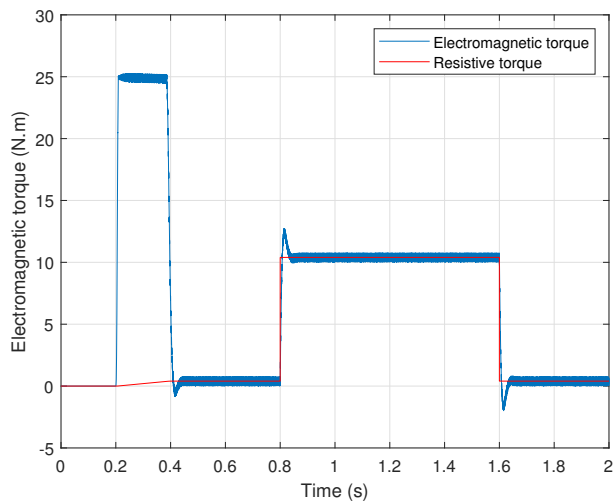
The proposed twelve-sector DTC with the ANN switching table and fuzzy logic control was proven to have good performance characteristics in terms of rapidity, robustness, and harmonic reduction. The response time was quicker and not sensitive to the load application, and the torque, flux, and current harmonics were reduced significantly.



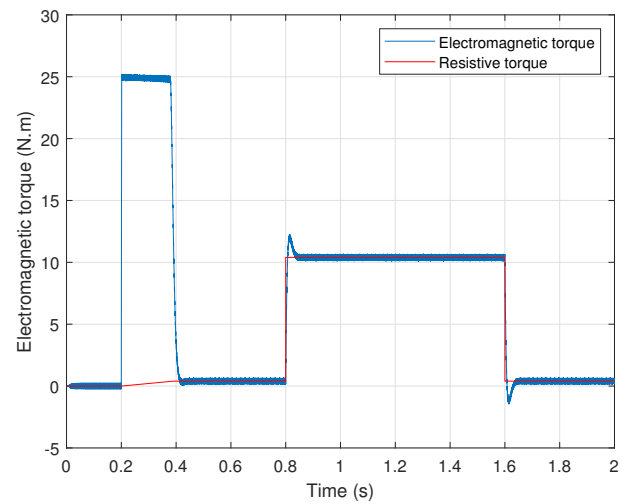
(a)



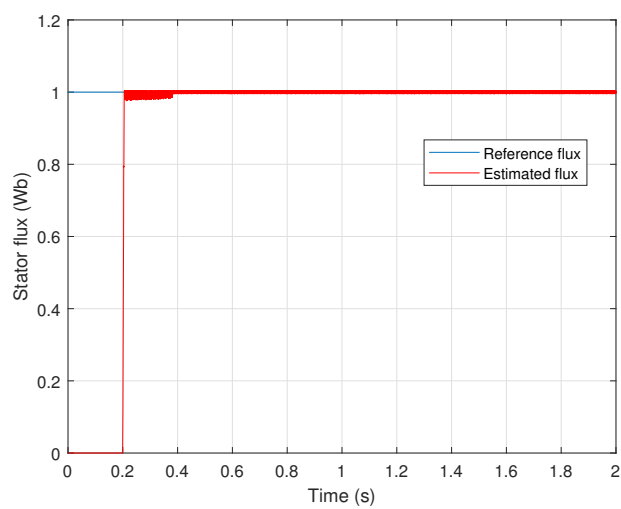
(b)



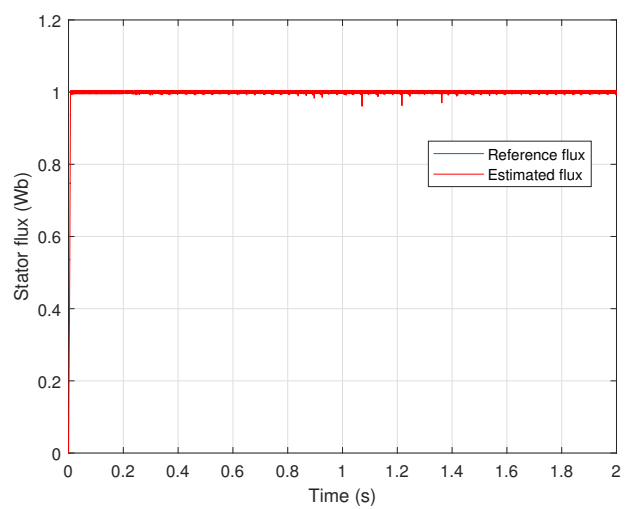
(c)



(d)



(e)



(f)

Figure 8. Cont.

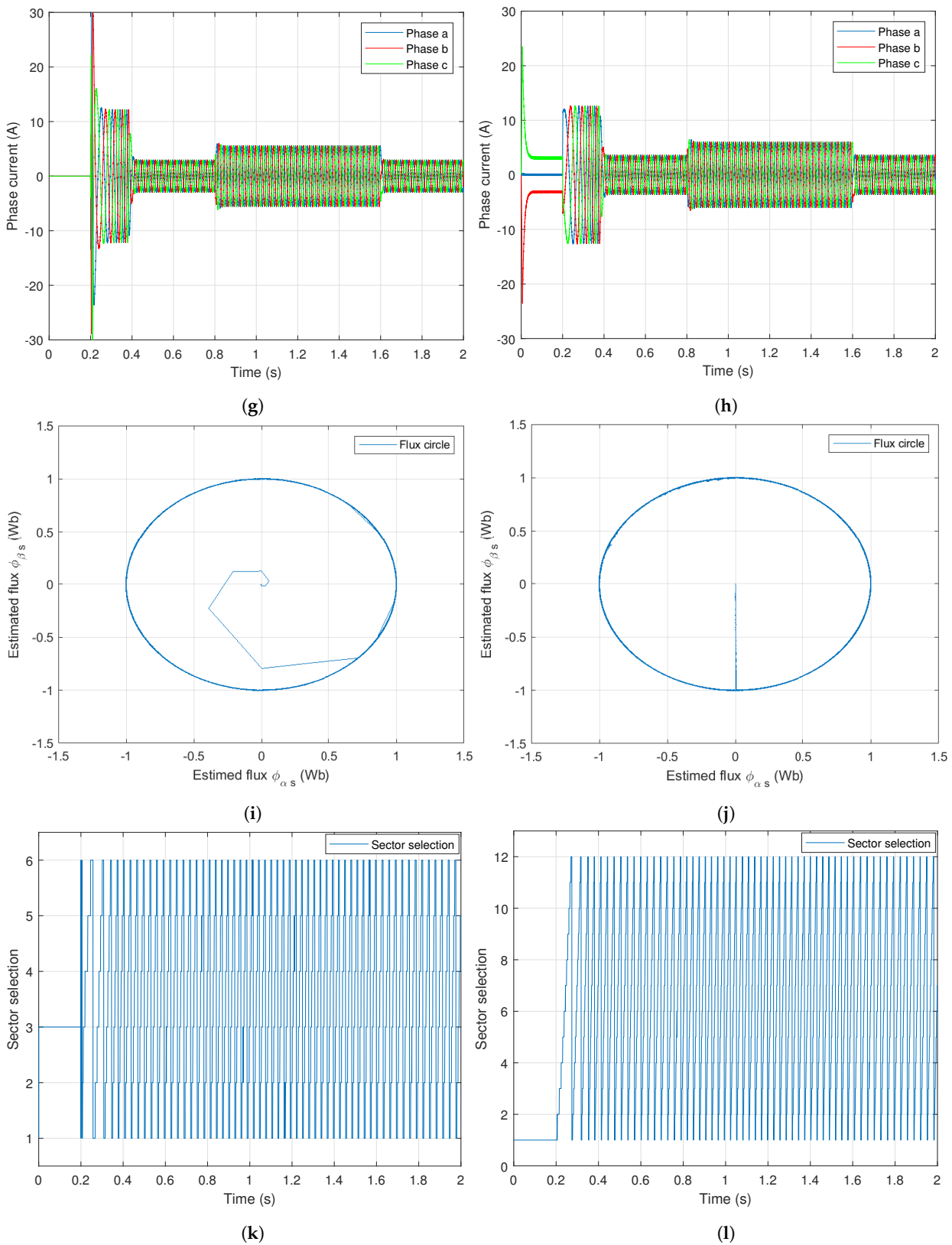


Figure 8. Improvement of DTC performance: start-up and steady-state with load application. (a) Basic DTC: mechanical speed, (b) proposed DTC: mechanical speed, (c) basic DTC: electromagnetic torque, (d) proposed DTC: electromagnetic torque, (e) basic DTC: stator flux linkage, (f) proposed DTC: stator flux linkage, (g) basic DTC: current of stator phase, (h) proposed DTC: current of stator phase, (i) basic DTC: circular trajectory of stator flux, (j) proposed DTC: circular trajectory of stator flux, and (k) basic DTC: sector selection, (l) proposed DTC: sector selection.

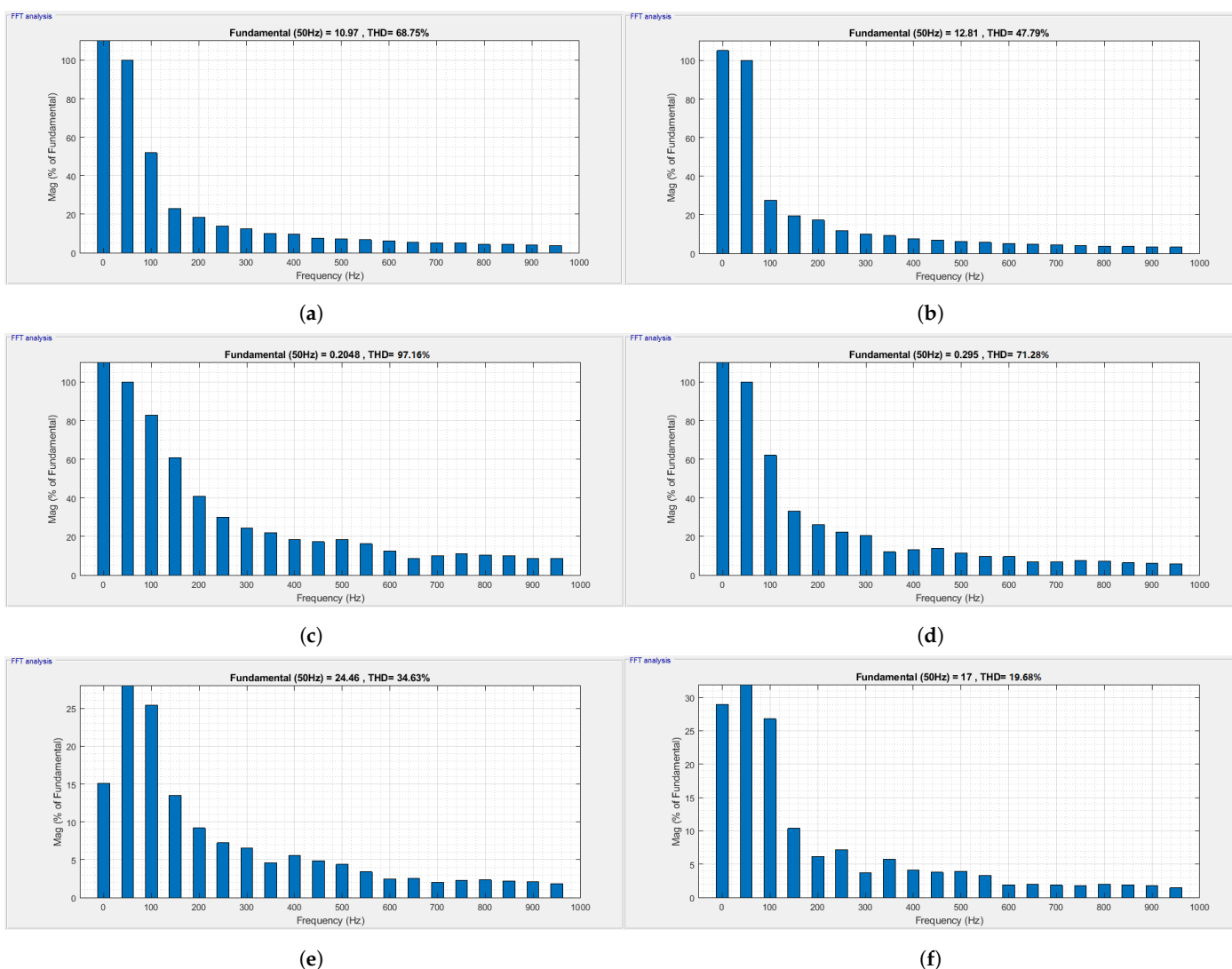


Figure 9. THD improvement of electromagnetic torque, stator flux linkage, and stator phase current. (a) Basic DTC: electromagnetic torque THD, (b) proposed DTC: electromagnetic torque THD, (c) basic DTC: flux of stator THD, (d) proposed DTC: flux of stator THD, (e) basic DTC: phase current THD, and (f) proposed DTC: phase current THD.

8. Conclusions

The design and simulation of improved DTC for induction motor operation were explained. Overall, the proposed method can make the system perform dynamically well while being operated at an instant step speed reference. When a load was applied suddenly to the system’s simulation, the system responded well, which indicates faster dynamics. The novel improvisation technique was also proven to give finer torque pulsation, flux distortion, and phase current pulsation. The flux ripples were reduced; magnitude tracking had a faster start-up; the waveforms had better components than the conventional DTC system response. Based on the experimental results, a system implemented with the proposed method was highly efficient and precise; the addition of the ANN-based switching table and the number of sectors played a critical role in the augmented system’s performance. However, the controllers must be very fast. Indeed, the reference voltages should be delivered very regularly to the ANN switching table to prevent any exceeding of the flux or the torque boundaries.

To ameliorate the performance of the DTC scheme, a new twelve-sector ANN switching table was presented in this paper. The speed, flux, and torque loops were controlled by

robust fuzzy logic regulators against external load torque. At an instant speed, the system harmonics level was reduced; the flux circular trajectory was enhanced.

Author Contributions: Conceptualization, C.F., Y.Z. and M.K.; Data curation, M.A., E.E.E. and S.K.; Formal analysis, M.K. and M.A.; Resources, C.F., Y.Z., M.A. and E.E.E.; Methodology, C.F., Y.Z., M.K. and M.A.; Software, C.F. and Y.Z.; Supervision, M.A. and S.K.; Validation, C.F., Y.Z. and M.A.; Visualization, M.A., M.K. and E.E.E.; Writing—original draft, C.F., Y.Z. and M.K.; Writing—review & editing, M.A., E.E.E. and S.K. All authors together organized and refined the manuscript in the present form. All authors have approved the final version of the submitted paper. All authors have read and agreed to the published version of the manuscript.

Funding: This work was supported by Taif University Researchers Supporting Project number (TURSP-2020/86): Taif University, Taif, Saudi Arabia.

Institutional Review Board Statement: Not applicable.

Informed Consent Statement: Not applicable.

Data Availability Statement: Not applicable.

Conflicts of Interest: The authors declare no conflict of interest.

Appendix A

Table A1. The machine used in the simulation: rated power and parameters.

Power	3 kW
Mechanical speed	1440 rpm
Pole pairs number	2
Frequency	50 Hz
Rated voltage	220/380 V
Rated current	12.5/7.2 A
Resistance of stator	2.20 Ω
Resistance of rotor	2.680 Ω
Inductance of stator	0.2290 H
Inductance of rotor	0.2290 H
Mutual inductance	0.2170 H
Moment of inertia	0.0470 kg·m ²
Coefficient of viscous friction	0.0040 N·s/rad

References

- Saad, N.; Irfan, M.; Ibrahim, R. *Condition Monitoring and Faults Diagnosis of Induction Motors: Electrical Signature Analysis*; CRC Press: New York, NY, USA, 2018.
- Thomson, W.T.; Culbert, I. *Current Signature Analysis for Condition Monitoring of Cage Induction Motors: Industrial Application and Case Histories*; John Wiley & Sons: Hoboken, NJ, USA, 2017.
- Faiz, J.; Ghorbanian, V.; Joksimovic, G. *Fault Diagnosis of Induction Motors*; Institution of Engineering and Technology: Westminster, UK, 2017.
- Dybkowski, M.; Klimkowski, K. Artificial Neural Network Application for Current Sensors Fault Detection in the Vector Controlled Induction Motor Drive. *Sensors* **2019**, *19*, 571. [[CrossRef](#)] [[PubMed](#)]
- Zahraoui, Y.; Akherraz, M.; Fahassa, C.; Elbadaoui, S. Robust control of sensorless sliding mode controlled induction motor drive facing a large scale rotor resistance variation. In Proceedings of the SCA'19, 4th International Conference on Smart City Applications, Casablanca, Morocco, 2–4 October 2019; Association for Computing Machinery: New York, NY, USA, 2019; pp. 1–6.
- Salem, F.B. *Direct Torque Control Strategies of Electrical Machines*; IntechOpen: London, UK, 2021.
- Wang, F.; Zhang, Z.; Mei, X.; Rodríguez, J.; Kennel, R. Advanced Control Strategies of Induction Machine: Field Oriented Control, Direct Torque Control and Model Predictive Control. *Energies* **2018**, *11*, 120. [[CrossRef](#)]
- Kumar, R.H.; Iqbal, A.; Lenin, N.C. Review of recent advancements of direct torque control in induction motor drives—A decade of progress. *IET Power Electron.* **2017**, *11*, 1–15. [[CrossRef](#)]
- Satpathy, S.R.; Pradhan, S.; Pradhan, R.; Sahu, R.; Biswal, A.P.; Ganthia, B.P. Direct Torque Control of Mathematically Modeled Induction Motor Drive Using PI-Type-I Fuzzy Logic Controller and Sliding Mode Controller. In *Intelligent Systems*; Udgata, S.K., Sethi, S., Srirama, S.N., Eds.; Lecture Notes in Networks and Systems; Springer: Singapore, 2021; pp. 239–251.
- Ammar, A.; Talbi, B.; Ameid, T.; Azzoug, Y.; Kerrache, A. Predictive direct torque control with reduced ripples for induction motor drive based on T-S fuzzy speed controller. *Asian J. Control* **2019**, *21*, 2155–2166. [[CrossRef](#)]

11. Zhang, Z.; Wei, H.; Zhang, W.; Jiang, J. Ripple Attenuation for Induction Motor Finite Control Set Model Predictive Torque Control Using Novel Fuzzy Adaptive Techniques. *Processes* **2021**, *9*, 710. [[CrossRef](#)]
12. Essalmi, A.; Mahmoudi, H.; Abbou, A.; Bennassar, A.; Zahraoui, Y. DTC of PMSM based on artificial neural networks with regulation speed using the fuzzy logic controller. In Proceedings of the 2014 International Renewable and Sustainable Energy Conference (IRSEC), Ouarzazate, Morocco, 17–19 October 2014; pp. 879–883.
13. Ayrir, W.; Haddi, A. Fuzzy 12 sectors improved direct torque control of a DFIG with stator power factor control strategy. *Int. Trans. Electr. Energy Syst.* **2019**, *29*, e12092. [[CrossRef](#)]
14. Fahassa, C.; Akherraz, M.; Zahraoui, Y. ANFIS-based hysteresis comparators with intelligent dual observer and speed controller of a direct torque control. *Int. J. Powertrains* **2020**, *9*, 150. [[CrossRef](#)]
15. Roman, R.C.; Precup, R.E.; Petriu, E.M. Hybrid data-driven fuzzy active disturbance rejection control for tower crane systems. *Eur. J. Control* **2021**, *58*, 373–387. [[CrossRef](#)]
16. Zhu, Z.; Pan, Y.; Zhou, Q.; Lu, C. Event-Triggered Adaptive Fuzzy Control for Stochastic Nonlinear Systems With Unmeasured States and Unknown Backlash-Like Hysteresis. *IEEE Trans. Fuzzy Syst.* **2021**, *29*, 1273–1283. [[CrossRef](#)]
17. Wang, K.; Huai, R.; Yu, Z.; Zhang, X.; Li, F.; Zhang, L. Comparison Study of Induction Motor Models Considering Iron Loss for Electric Drives. *Energies* **2019**, *12*, 503. [[CrossRef](#)]
18. Doncker, R.W.D.; Pülle, D.W.J.; Veltman, A. *Advanced Electrical Drives: Analysis, Modeling, Control*; Springer Nature: Cham, Switzerland, 2020.
19. Karlovsky, P.; Lettl, J. Induction Motor Drive Direct Torque Control and Predictive Torque Control Comparison Based on Switching Pattern Analysis. *Energies* **2018**, *11*, 1793. [[CrossRef](#)]
20. Hakami, S.S.; Mohd, A.I.; Lee, K.B. Low-Speed Performance Improvement of Direct Torque Control for Induction Motor Drives Fed by Three-Level NPC Inverter. *Electronics* **2020**, *9*, 77. [[CrossRef](#)]
21. Zahraoui, Y.; Akherraz, M.; Elbadaoui, S. Fuzzy Logic Speed Control and Adaptation Mechanism-Based Twelve Sectors DTC to Improve the Performance of a Sensorless Induction Motor Drive. *Int. J. Electr. Eng. Inform.* **2021**, *13*, 508–529. [[CrossRef](#)]
22. Pal, A.; Srivastava, G.D.; Kulkarni, R.D. Simulation of Sensorless Speed Control of Induction Motor Using Direct Torque Control Technique Employing Five Level Torque Comparator and Twelve Sector Method. In Proceedings of the 2019 International Conference on Nascent Technologies in Engineering (ICNTE), Navi Mumbai, India, 4–5 January 2019; pp. 1–6.
23. Mejia-Barron, A.; de Santiago-Perez, J.J.; Granados-Lieberman, D.; Amezcua-Sanchez, J.P.; Valtierra-Rodriguez, M. Shannon Entropy Index and a Fuzzy Logic System for the Assessment of Stator Winding Short-Circuit Faults in Induction Motors. *Electronics* **2019**, *8*, 90. [[CrossRef](#)]
24. Fahassa, C.; Akherraz, M.; Zahraoui, Y. ANFIS Speed Controller and Intelligent Dual Observer Based DTC of an Induction Motor. In Proceedings of the 2018 International Symposium on Advanced Electrical and Communication Technologies (ISAECT), Rabat, Morocco, 21–23 November 2018; pp. 1–6.
25. Skowron, M.; Wolkiewicz, M.; Orłowska-Kowalska, T.; Kowalski, C.T. Application of Self-Organizing Neural Networks to Electrical Fault Classification in Induction Motors. *Appl. Sci.* **2019**, *9*, 616. [[CrossRef](#)]
26. Benbouhenni, H. Seven-Level Direct Torque Control of Induction Motor Based on Artificial Neural Networks with Regulation Speed Using Fuzzy PI Controller. *Iran. J. Electr. Electron. Eng.* **2018**, *14*, 85–94.
27. Mekrini, Z.; Bri, S. High—Performance using Neural Networks in Direct Torque Control for Asynchronous Machine. *Int. J. Electr. Comput. Eng. (IJECE)* **2018**, *8*, 1010–1017. [[CrossRef](#)]